Compressed Ultrafast Electron Diffraction Imaging Through Electronic Encoding

Dalong Qi,[1] Chengshuai Yang,[1] Fengyan Cao,[1] Jinyang Liang,[2] Yilin He,[1] Yan Yang,[1] Tianqing Jia,[1] Zhenrong Sun,[1,*] and Shian Zhang[1,3,†]

[1] *State Key Laboratory of Precision Spectroscopy, School of Physics and Materials Science, East China Normal University, 3663 North Zhongshan Road, Shanghai 200062, P. R. China*

[2] *Centre Énergie Matériaux Télécommunications, Institut National de la Recherche Scientifique, 1650 boulevard Lionel-Boulet, Varennes, QC J3X1S2, Canada*

[3] *Collaborative Innovation Center of Extreme Optics, Shanxi University, Taiyuan 030006, P. R. China*

(Received 1 April 2018; revised manuscript received 3 September 2018; published 28 November 2018)

Ultrafast electron diffraction (UED) with high temporal and spatial resolutions is a powerful tool to observe transient structural changes in materials on an atomic scale. This technique is based on a pump-probe method using ultrashort laser and electron pulses. Therefore, UED requires that the measured transients be highly repeatable. Moreover, the relative time jitter between laser and electron pulses significantly affects the UED temporal resolution. To overcome the UED technical limitations, we propose a technique called compressed ultrafast electron diffraction imaging (CUEDI). In this technique, we encode time-evolving electron diffraction patterns with random codes on an electron encoder. Then, the encoded electron diffraction pattern is measured by a detector after a temporal shearing operation. Finally, the evolution process of the electron diffraction pattern is reconstructed using a compressed sensing algorithm. We confirm the feasibility of our proposed scheme by numerically simulating the polycrystalline gold melting process based on the experimental data measured with the pump-probe method. Because CUEDI employs a continuous or long electron pulse, the relative time jitter between laser and electron pulses can be eliminated. Additionally, CUEDI measures transients with a single shot, which allows irreversible processes to be directly observed.

DOI: 10.1103/PhysRevApplied.10.054061

I. INTRODUCTION

Directly observing ultrafast structural dynamics on an atomic scale is a challenge in solid-state physics, chemical reactions, and biology. Therefore, researchers have developed various techniques to achieve this goal, and ultrafast electron diffraction (UED) has been proposed as a useful technique to resolve real-time structural dynamics of matter [1,2]. In the UED system, an ultrashort pulsed laser is used to generate an electron pulse, and a pump-probe protocol is employed. In the experiment, an ultrashort laser pulse excites the measured sample to a far-from-equilibrium state, and an ultrafast electron pulse is used to probe variable delayed points in the relaxation pathway to unravel the structural dynamics. Because of its larger scattering cross section, smaller probe beam energy deposition, and compact table-top design, UED has advantages over x-ray-based structural analysis techniques [2,3]. In the past decade, a variety of UED techniques and facilities have made tremendous progress [4–8], and several experiments have been performed to obtain atomically resolved dynamics of elementary substances [9–12], metallic compounds [13–15], and organic complexes [16]. In UED experiments, the electron number per pulse is tunable, but each electron pulse usually needs to contain enough (usually at least 10^5) electrons to minimize the data acquisition time. Based on UED, the structural dynamics of a variety of molecules in both crystal and gas phases have been explored. In the crystal, the phase transition phenomena, including charge density waves, charge transfer, and spin crossover, have been experimentally observed [14,15,17,18]. In the gas phase molecule, the transient structures in chemical reaction, as well as coherent nuclear motion, were studied to obtain molecular movies of complex chemical reactions [19,20]. So far, UED has become a powerful tool to observe real-time structural dynamics.

To use a stroboscopic procedure to resolve the structural dynamics, an ultrashort and intense electron pulse is needed to provide an adequate instrumental response resolution. Therefore, generating an electron pulse that is short while still containing a large quantity of electrons is a desirable development for UED. However,

*zrsun@phy.ecnu.edu.cn
†sazhang@phy.ecnu.edu.cn

the space-charge effect (SCE) between charged electrons, which will broaden the electron pulse, is an obstacle. Radio frequency (rf) technology was introduced to compress the electron pulse to the initial duration [4], but the arrival time jitter between the electron pulse and rf field has always inhibited the ability to obtain the shorter electron pulse. In previous studies with the stroboscopic technique, the experiments were performed with a multiple-shot arrangement by varying the time delay between the pump laser pulse and probe electron pulse [9–20]. Recently, a scheme combining a long probe electron pulse with a time-resolving streaking was proposed to realize a single shot measurement [21,22], but this technique was limited to the measurement of some special single-crystalline samples. Moreover, a computational image reconstruction method based on Bayesian analysis was proposed to recover the smearing diffraction pattern [23]; however, this method has insufficient constraints to uniquely invert the powder/symmetric diffraction patterns. To date, the realization of a true single-shot imaging for various structural dynamics is still challenging.

We propose a technique called compressed ultrafast electron diffraction imaging (CUEDI). In this technique, the dynamical evolution scene is reconstructed by image encoding and decoding based on compressed sensing (CS), which can overcome the current UED technical limitations. In CUEDI, a time-resolved electron diffraction data cube is encoded by an electron encoder, deflected by a time-varying electric field, and recorded by a detector, and finally the two-dimensional (2D) superimposed data are decoded by CS algorithm to recover the time-evolving electron diffraction pattern. To validate the feasibility of our proposed scheme, a detailed electron trajectory is simulated using a charged particle-tracing software, and a time-resolved electron diffraction pattern for the polycrystalline gold melting process is reconstructed based on the CS algorithm. The simulation and reconstruction results indicate that CUEDI is capable of resolving the structural dynamics in reciprocal space with one shot, and has great potential to replace the traditional pump-probe scheme.

II. BASIC PRINCIPLE

The CUEDI schematic diagram is shown in Fig. 1(a). First, a magnetic lens is used to collimate the diffracted electron beam in space, and an electron encoder is designed to encode the time-evolving electron diffraction pattern. Then, the encoded electron diffraction pattern data cube is measured by a detector after a temporal shearing operation. Finally, the evolution process of the electron diffraction pattern is reconstructed by a CS algorithm. In the transmissive experimental design, the measured sample is instantaneously stimulated to an excited state by an ultrashort pulsed laser. Simultaneously, a long, flat-top pulsed laser, i.e., a duration of hundreds of nanoseconds, or a continuous laser with sufficient photon energy is employed to strike the photocathode material (such as a metal film) to generate an electron source. A cold-atom electron source is more suitable under these conditions because it has a higher brightness and longer transversal coherence length [24,25]. The electron source is then accelerated by a static electric field for continuous probe. After scattering with the atomic array in the measured sample, the diffracted electron beam moves forward to the electron encoder for random encoding. Finally, the encoded and time-varying electron diffraction pattern is converted from the time domain to the space domain by a time-dependent electric field and recorded by the detector.

The electron encoder is designed as a 2D random-distribution plane, which is composed of many microchannel tubes that originate from microchannel plates (MCP), and the electron encoder prototype is shown in Fig. 1(b). The MCP-like encoder is divided into a number of square

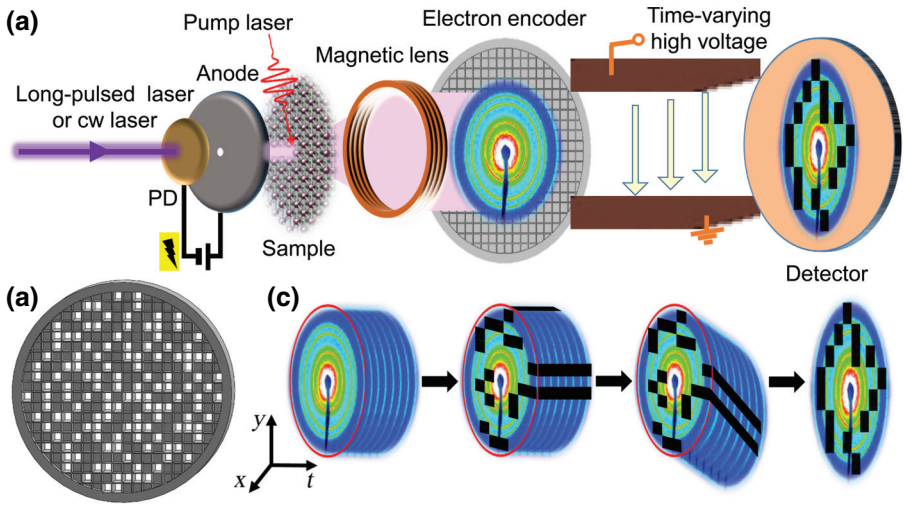

FIG. 1. The schematic diagram of the compressed ultrafast electron diffraction imaging (a), PD: photocathode; a detailed illustration of the electron encoder (b); the data acquisition for the compressed ultrafast electron diffraction imaging (c).

tubes. The gray tubes denote the micro-Faraday cups that block the electrons, and the white ones are the microchannel tubes that allow the electrons to pass. To clarify, the designed electron encoder here is just used as a mask, and therefore, there is no secondary electron generation in order to retain the temporal information of the diffracted electron beam.

The data acquisition of the electron diffraction pattern in CUEDI is shown in Fig. 1(c). First, the electron beam is diffracted by the measured sample, which can be expressed as $I(x,y,t)$, where x and y represent spatial coordinates and t represents the temporal coordinate. Second, the electron diffraction pattern is encoded by a spatial encoding operator, C, followed by a temporal shearing operator, S. Finally, the encoded electron diffraction pattern is recorded by a detector, such as a CCD, to generate an optical energy $E(x,y)$. By introducing a spatial-temporal integration operator, T, to temporally integrate over the exposure time in each CCD pixel, $E(x,y)$ can be expressed as

$$E(x,y) = TSCI(x,y,t). \tag{1}$$

To reconstruct the original time-evolving electron diffraction pattern $I(x,y,t)$, one needs to inversely solve Eq. (1). Based on measured $E(x,y)$ and operators T, S, and C given above, the transient data cube, $I(x,y,t)$, can be reconstructed using a CS algorithm. Here, a two-step iterative shrinkage/thresholding (TwIST) algorithm is employed [26], which is used to locate the minimal value of the following object function, as shown below

$$f_{\mathrm{TwIST}} = \arg\min \left\{ \frac{1}{2} ||E(x,y) - TSCI(x,y,t)||_2^2 + \beta \Phi[I(x,y,t)] \right\}, \tag{2}$$

where β is the regularization parameter and $\Phi(I(x,y,t)$ is the regularization function that can be written as

$$\begin{aligned} \Phi(X) = & \sum_{k=1}^{N_z} \sum_{i=1}^{N_x \times N_y} \sqrt{(\Delta_i^h X_k)^2 + (\Delta_i^v X_k)^2} \\ & + \sum_{m=1}^{N_y} \sum_{i=1}^{N_x \times N_z} \sqrt{(\Delta_i^h X_m)^2 + (\Delta_i^v X_m)^2} \\ & + \sum_{n=1}^{N_x} \sum_{i=1}^{N_y \times N_z} \sqrt{(\Delta_i^h X_n)^2 + (\Delta_i^v X_n)^2}, \end{aligned} \tag{3}$$

where N_x and N_y are the row and column pixel numbers in each image, respectively; N_z is the image number; m, n, and k are the three indices; X_k, X_m, and X_n represent the 2D datum along the three indices k, m, and n, respectively; and Δ_i^h Δ_i^v are the horizontal and vertical first-order local difference operators on the 2D datum, respectively. In the image reconstruction, as shown in Eq. (2), the minimization of the first term $||E(x,y) - TSCI(x,y,t)||$ is used to obtain maximal matching between the estimated measurement $TSCI(x,y,t)$ and the actual measurement $E(x,y)$, whereas the minimization of the second term $\beta\Phi(I(x,y,t))$ is used to encourage $I(x,y,t)$ to be piecewise constant, where the regularization parameter β controls the relative weight of the two terms and obtains an almost identical physical reality.

III. RESULTS AND DISCUSSION

To generate an electron diffraction pattern with a sufficiently high SNR, more than 10^6 electrons are required. Thus, SCE plays an important role in the propagation process of the electron beam. In CUEDI, we use a long-pulsed or continuous electron beam as the probe, thus the temporal broadening of the electron beam can be less considered. However, the spatial broadening due to the electronic encoding needs to be dealt with in detail. To identify how SCE affects this process, a charged-particle simulation software, SIMION 8.0 (Scientific Instrument Services, Ringoes, NJ, USA), is used to trace the propagation trajectory of the electron beam after the encoder without deflection. Here, two typical electron diffraction patterns, i.e., concentric rings for polycrystals (PCs) and Bragg spots for single crystals (SCs), are considered for the simulation, as shown in Figs. 2(a) and 2(b), respectively. For simplicity, a tiny quadrangle region across the ring is selected on a PC-diffraction pattern, and a unit code array with five rows and three columns is applied to this region. Here, the unit code size is $500 \times 500\,\mu\mathrm{m}^2$. Thus, the electrons in this region are divided into a series of beamlets. In the following discussion, the PC case is used as an example for the simulation, and the same results can be observed for the SC case. In our simulation, the initial parameters are listed in Table I. As shown in Fig. 2(a), the electrons in the specified region appear as a Gaussian distribution in the space. These electron beamlets after the encoder are shown in the left panel of Fig. 2(c) and are labeled from A to O, respectively. In these electron beamlets, each blue spot represents a flying electron. In each column, the five electron beamlets contain 200, 600, 1000, 600, and 200 electrons, respectively. Thus, the maximum and minimum electron densities can be calculated as 4000/ and 800/mm^2, respectively. The electron beamlets at the detector position are shown in the right panel of Fig. 2(c). By comparing the transverse distribution of these electron beamlets at the initial and final positions, an obvious expansion can be observed, especially for those electron beamlets with the higher electron density. To quantitatively assess this expansion, the electron beamlet size along the x and y directions at the encoder and detector positions are compared. Here, the expansion coefficient is defined as

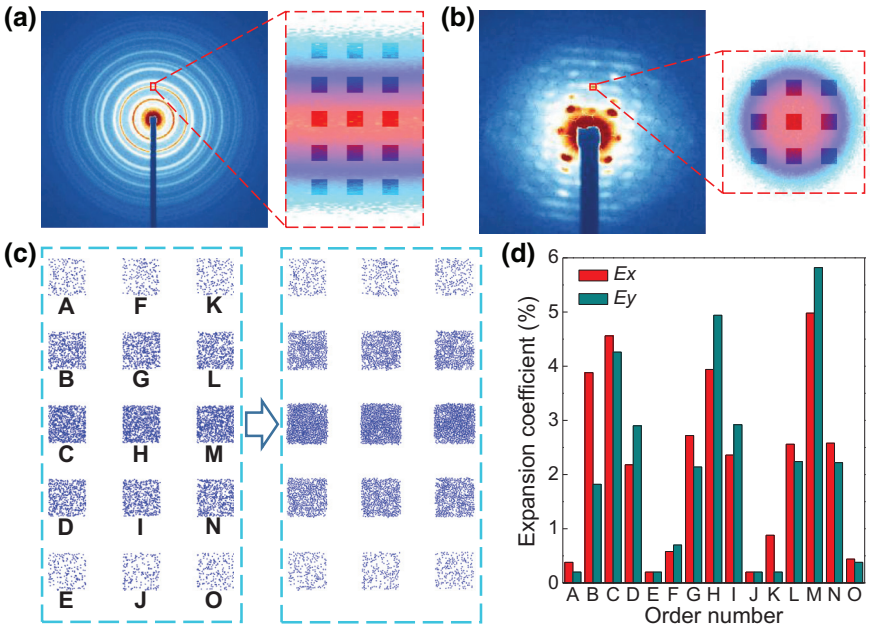

FIG. 2. The electron diffraction patterns for poly (a) and single (b) crystals with the enlarged region across a Bragg ring or spot; the encoded diffraction patterns on the electron encoder (left panel) and the CCD detector (right panel) (c); the expansion coefficients of the electron beamlets along the x and y directions E_x and E_y (d).

$E = (L_{\text{fin}}\text{-}L_{\text{ini}})/L_{\text{ini}}$, where L_{ini} and L_{fin} are the length in the x direction or width in the y direction of the electron beamlet at the initial and final positions. The expansion coefficients E_x and E_y of all the electron beamlets are shown in Fig. 2(d). A quasi-isotropy expansion in each electron beamlet can be observed. The average expansion coefficient is almost 5% for the stronger electron beamlets (C, H, and M), while it is approximately just 0.5% for the weaker electron beamlets (A, F, K, E, J, and O). These electron beamlets expand in the space due to SCE, but their relative positions remain unchanged. Therefore, the electron beamlet expansion should be due to intrabeamlet SCE, and interbeamlet SCE has no contribution to the expansion.

In CUEDI, the modulated code pattern on the CCD detector is used to reconstruct the time-evolving electron diffraction pattern, but not the unit code pattern on the encoder. Here, the modulated code pattern is obtained by measuring the encoded electron diffraction pattern on the detector. The electron density, unit code size, and kinetic energy are three important parameters that affect the modulated code pattern due to the electron beamlet expansion. To analyze the effect of the three parameters on the electron beamlet expansion, we fix two parameters and vary the third parameter. Without the special illustration, the initial parameters are given in Table I. The expansion coefficients for the stronger electron beamlet in Fig. 2(c) under the three cases are shown in Fig. 3. As shown in Fig. 3(a), the electron beamlet experiences an almost linear expansion with an increase in the electron density. When the electron density increases to 20 000/mm^2, the expansion coefficients in both the x and y directions reach approximately 25%. In this case, the electron beamlets are greatly affected by intrabeamlet SCE, which will probably cause the time-evolving electron diffraction pattern to not be correctly reconstructed. As shown in Fig. 3(b), the expansion coefficient decreases when the unit code size increases. If the unit code size increases to more than 800 $\times$ 800 μm^2, the expansion coefficient can decrease to less than 4%, which is very beneficial for the image reconstruction of the electron diffraction pattern. Moreover, as shown in Fig. 3(c), the expansion coefficient shows a fast decrease followed by a slow decrease process with the increase of the kinetic energy of the electron beam. When the kinetic energy reaches 150 keV or higher, the expansion coefficients along both x and y directions are kept within 1%. The simulation results can provide important guidance for the electron density, kinetic energy, and electron encoder designs in the experiment.

When the crystal sample is excited by the pump-pulsed laser, the electron beamlet sizes will correspondingly change due to the electron density variation, and a dynamically modulated code pattern is formed. In the experiment, the dynamically modulated code pattern cannot be measured. Here, we use a fixed modulated code pattern without the pump-laser excitation for the image reconstruction. Usually, the electron density varies in the range of 40% when the crystal phase changes. Such a scale can cover the electron density variation in most UED experiments

TABLE I. The initial simulation parameters.

Total particle number	7800
Mass per particle (a.u.)	$5.485\,799\,03 \times 10^{-4}$
Kinetic energy (eV)	30 000
Flight distance (mm)	400
Unit code size (μm^2)	500 $\times$ 500
Electron density (/mm^2)	4000

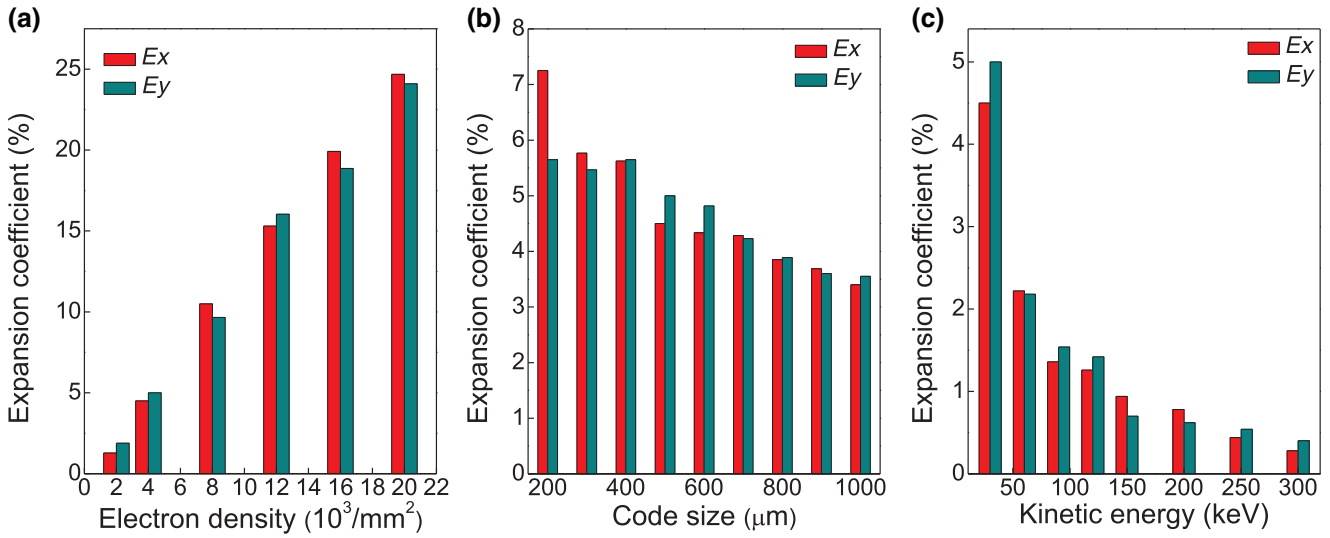

FIG. 3. The expansion coefficients along the x and y directions E_x and E_y with varying electron density (a), unit code size (b), and kinetic energy (c).

[9–17]. As shown in Figs. 2(c) and 2(d), 40% electron density variation has no obvious effect on the electron beamlet expansion, such as the two patterns with the electron densities from 4000 (C, H, and M) to 2400/mm^2 (B, G, and L). To show that the fixed modulated code pattern can be used to reconstruct the time-evolving electron diffraction pattern, we reconstruct the pattern in the specified region of Fig. 2(a) with the normalized intensity attenuation from 1 to 0.6, as shown in Fig. 4(a). Here, a total of twelve patterns are considered, which are labeled from t_0 to t_{11} according to the time sequence, respectively. Similar to the image operation in Fig. 1(c), these patterns are randomly encoded and superimposed in sequence to form a new pattern, where each pattern is shifted by a pixel in the space along the vertical direction relative to the previous pattern. The reconstruction results by the TwIST algorithm are shown in Fig. 4(b). By comparing Figs. 4(a) and 4(b), it can be seen that both the spatial intensity distribution and temporal intensity evolution are recovered well. For quantitatively identifying the fidelity of these reconstructed

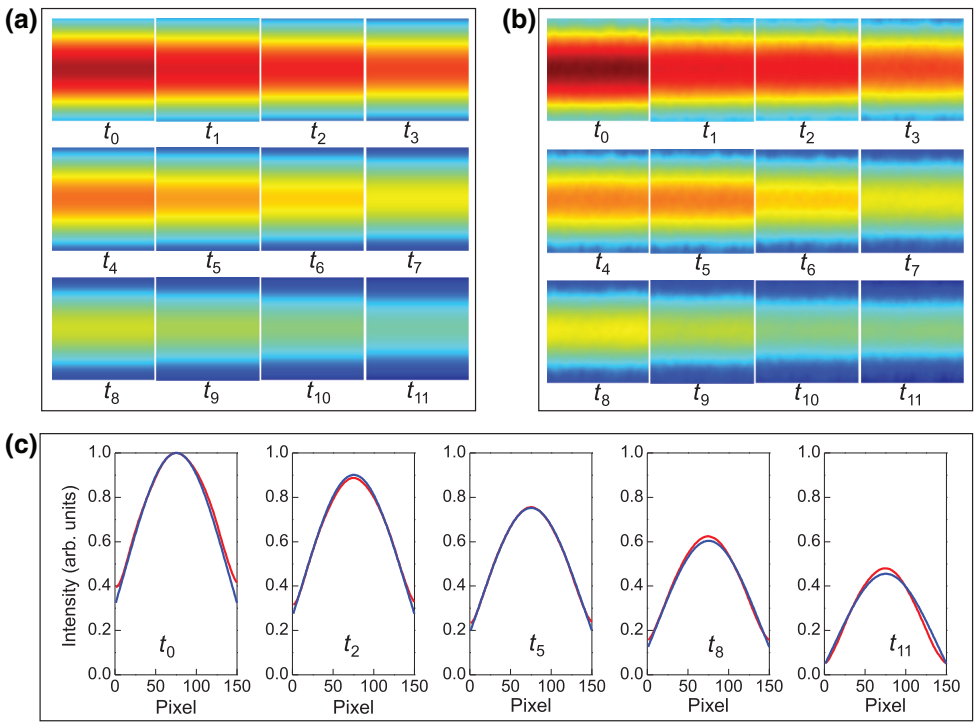

FIG. 4. The original (a) and reconstructed (b) electron diffraction patterns in the specified region of Fig. 2(a) with the intensity attenuation; The normalized spatial intensity distributions of original (blue lines) and reconstructed (red lines) patterns with the time sequences of t_0, t_2, t_5, t_8, and t_{11} (c).

patterns, the normalized spatial intensity distributions of original and reconstructed patterns with the time sequences of t_0, t_2, t_5, t_8, and t_{11} are shown in Fig. 4(c). Obviously, the reconstructed patterns highly replicate the intensity information from the original patterns. In our method using the image encoding and decoding, a too high or low encoding percentage (i.e., the percentage of the encoding part in the whole image) is not beneficial for the image reconstruction. Based on our simulation, encoding percentages in the range of 40%–60% have higher image reconstruction accuracy. In the experiment, the encoding percentage is proposed at around 50%.

To further validate the CS-based image reconstruction robustness in CUEDI, a number of time-resolved electron diffraction patterns in the polycrystalline gold melting process is chosen for the image reconstruction. Here, these electron diffraction patterns are obtained by experimental measurement with the pump-probe method [14]. The original fifteen electron diffraction patterns with a time step of 2 ps are shown in Fig. 5(a), and one enlarged diffraction pattern with a delay time of 2 ps and its radial intensity distribution are shown in Figs. 5(b) and 5(c), respectively. These main diffraction peaks can be clearly resolved, as shown in Fig. 5(c), which represent the lattice planes

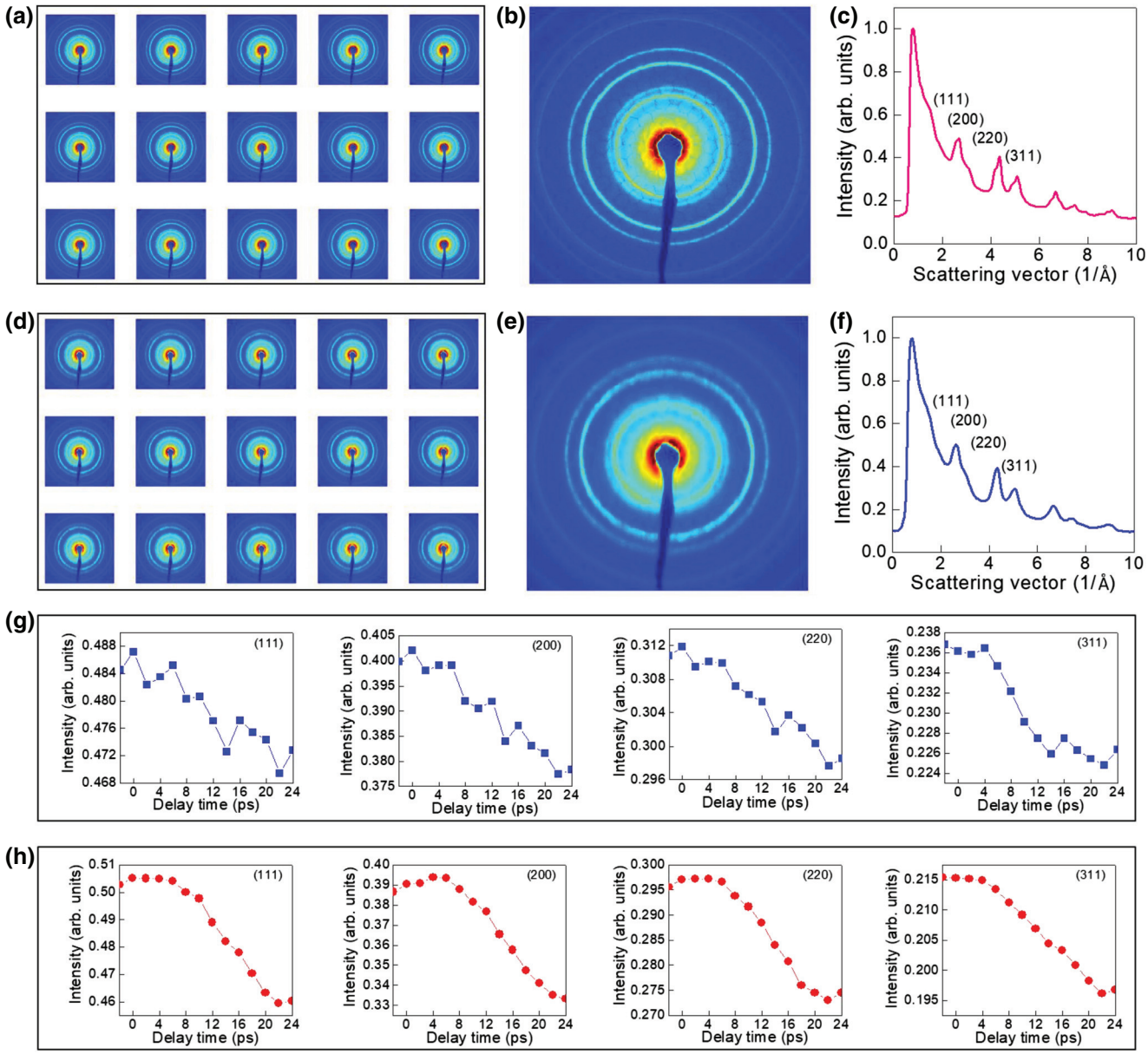

FIG. 5. The original (a) and reconstructed (d) electron diffraction patterns for the polycrystalline gold melting process, together with the enlarged diffraction patterns for a delay time of 2 ps (b), (e) and their corresponding radial intensity distributions (c), (f); the original (g) and reconstructed (h) intensity evolutions of the four diffraction peaks (111), (200), (220), and (331).

along the scattering vector. Through the image reconstruction with the TwIST algorithm, the reconstructed electron diffraction patterns are shown in Fig. 5(d). Similarly, the selected diffraction pattern and its radial intensity distribution are also shown in Figs. 5(e) and 5(f), respectively. As shown in Fig. 5(e), the reconstructed diffraction pattern shows some blurring relative to the original pattern in Fig. 5(b), but the lattice planes can still be clearly resolved from the radial intensity distribution in Fig. 5(f). Additionally, the intensity evolutions of four diffraction peaks (111), (200), (220), and (311) are extracted from both the original and reconstructed diffraction patterns in Figs. 5(a) and 5(d), and the calculated results are shown in Figs. 5(g) and 5(h), respectively. As expected, the reconstructed intensity evolution traces maintain high reproducibility, but become smoother than the original traces.

As shown in Figs. 4 and 5, the CUEDI technique can provide a well-established tool to recover the time-evolving electron diffraction pattern with a single shot measurement. The achievable temporal resolution is the main concern for the experimental implementation. As shown in Fig. 1, the temporal resolution for CUEDI is mainly limited by the kinetic energy dispersion of the electron source, the time-varying voltage in the deflection plate, and the distance between the deflection plate and CCD detector. In our scheme, the electron source is generated by the long (ns or longer) laser pulse or continuous laser, which can ensure a uniform kinetic energy. In this case, all the electron velocities in the propagation process can reach a relatively balanced status, and thus the energy spread of the electrons due to the space charge effect is negligible. A similar case can be observed in the stretch of the ultrashort electron pulse [27]. When the electron pulse is significantly stretched, the axial velocity of the electrons is almost unchanged. That is to say, the kinetic energy of the electrons has basically no change in the propagation process. Therefore, the electron energy spread in our method almost does not affect the temporal resolution. Since the effect of the electron energy spread can be ignored and all the electrons have the same kinetic energy, the electron pulse width almost remains unchanged in the propagation process. Moreover, with the development of the photoswitch as well as a terahertz field, the temporal resolution can reach less than one hundred femtoseconds [28,29], which is high enough for streaking.

In the CUEDI scheme, the experiment is completed with a single shot measurement, and the long pulsed or continuous electron source is employed, therefore, there is no time jitter problem between the pump-laser pulse and probe electron beam, which is different from the traditional pump-probe scheme. However, the zero time is an important parameter that needs to be determined. One feasible method is to infer from the latter data based on the image reconstruction, i.e., the spatial position on the CCD detector, corresponding to the zero time, can be determined, but this method requires that the tested materials, such as antimony, gold, and so on, need to respond quickly under the pump-laser pulse excitation. In the sequent experiments, this zero time (or spatial position on the CCD detector) can be used as a benchmark. To ensure that the zero time is the same for the sequence measurements, the pump laser is required for frequency locking. Furthermore, the pump laser is also used to trigger the streak camera (i.e., deflection plate and CCD), and thus the pump laser and streak camera can be accurately synchronized.

IV. CONCLUSIONS

To conclude, we propose a computational ultrafast imaging technique, i.e., CUEDI, for UED based on a CS algorithm. In this technique, a time-evolving electron diffraction pattern is encoded by an electron encoder composed of randomly distributed microchannel tubes and micro-Faraday cups, then the encoded electron diffraction pattern is deflected by a time-varying electric field before being recorded by the detector, and finally a CS-based image reconstruction algorithm is employed to recover the evolution process of the electron diffraction pattern. The correct reconstruction of the time-evolving electron diffraction pattern for the polycrystalline gold melting process validates the feasibility of our proposed scheme. Compared with UED with a pump-probe scheme, CUEDI completes the experimental measurements in a single shot, which can eliminate the relative time jitter between the pump-laser pulse and the probe electron pulse. Furthermore, by introducing the CS algorithm, CUEDI needs requires fewer electrons, which can be reduced by about two orders of magnitude. Therefore, CUEDI may replace UED to be used in the study of real-time structural dynamics. This study shows that CUEDI can resolve the ultrafast dynamics on a picosecond time scale and has great potential for a higher temporal resolution. Moreover, this computational imaging method based on the CS algorithm not only has potential applications in the transmission electron microscopy (TEM) community, especially for time-dependent imaging in the emerging field of liquid cell TEM, but can also be extended to the x-ray regime to provide more possibilities for ultrafast structural imaging.

ACKNOWLEDGMENTS

This work was partially supported by the National Natural Science Foundation of China (Grants No. 11727810, No. 21603074, No. 11774094, No. 11804097, and No. 11474096), the Science and Technology Commission of Shanghai Municipality (Grants No. 17ZR146900, No. 16CG25, and No. 16520721200), and the Program of Introducing Talents of Discipline to Universities 111 Project No. B12024.

We thank the Miller group in Max-Planck Institute for the Structure and Dynamics of Matter to provide

the experimental setup for performing the pump-probe experiment in the polycrystalline gold melting process.

D.Q., C.Y., and F. C. contributed equally to this work.

[1] A. H. Zewail, 4D ultrafast electron diffraction, crystallography, and microscopy, Annu. Rev. Phys. Chem. **57**, 65 (2006).

[2] R. J. D. Miller, Femtosecond crystallography with ultrabright electrons and X-rays: Capturing chemistry in action, Science **343**, 1108 (2014).

[3] A. A. Ischenko, P. M. Weber, and R. J. D. Miller, Transient structures and chemical reaction dynamics, Russ. Chem. Rev. **86**, 1173 (2017).

[4] T. van Oudheusden, P. L. E. M. Pasmans, S. B. van der Geer, M. J. de Loos, M. J. van der Wiel, and O. J. Luiten, Compression of Subrelativistic Space-Charge-Dominated Electron Bunches for Single-Shot Femtosecond Electron Diffraction, Phys. Rev. Lett. **105**, 264801 (2010).

[5] M. Aidelsburger, F. O. Kirchner, F. Krausz, and P. Baum, Single-electron pulses for ultrafast diffraction, Proc. Natl. Acad. Sci. U.S.A. **107**, 19714 (2010).

[6] M. Gulde, S. Schweda, G. Storeck, M. Maiti, H. K. Yu, A. M. Wodtke, S. Schäfer, and C. Ropers, Ultrafast low-energy electron diffraction in transmission resolves polymers/graphene superstructure dynamics, Science **345**, 200 (2014).

[7] F. Fu, S. Liu, P. Zhu, D. Xiang, J. Zhang, and J. Cao, High quality single shot MeV electron diffraction from a photocathode radio-frequency gun, Rev. Sci. Instrum. **85**, 083701 (2014).

[8] S. P. Weathersby, G. Brown, M. Centurion, T. F. Chase, R. Coffee, J. Corbett, J. P. Eichner, J. C. Frisch, A. R. Fry, M. Guehr *et al.*, Mega-electron-volt ultrafast electron diffraction at SLAC national Accelerator Laboratory, Rev. Sci. Instrum. **86**, 073702 (2015).

[9] B. J. Siwick, J. R. Dwyer, R. E. Jordan, and R. J. D. Miller, An atomic view of melting using femtosecond electron diffraction, Science **302**, 1382 (2003).

[10] M. Harb, R. Ernstorfer, C. T. Hebeisen, G. Sciaini, W. Peng, T. Dartigalongue, M. A. Eriksson, M. G. Lagally, S. G. Kruglik, and R. J. D. Miller, Electronically Driven Structure Changes of Si Captured by Femtosecond Electron Diffraction, Phys. Rev. Lett. **100**, 155504 (2008).

[11] R. Ernstorfer, M. Harb, C. T. Hebeisen, G. Sciaini, T. Dartigalongue, and R. J. D. Miller, The formation of warm dense matter: Experimental evidence for electronic bond hardening in gold, Science **323**, 1033 (2009).

[12] G. Sciaini, M. Harb, S. G. Kruglik, T. Payer, C. T. Hebeisen, F. M. Heringdorf, M. Yamaguchi, M. H. Hoegen, R. Ernstorfer, and R. J. D. Miller, Electronic acceleration of atomic motions and disordering in bismuth, Nature **458**, 56 (2009).

[13] V. R. Morrison, R. P. Chatelain, K. Tiwari, A. Hendaoui, A. Bruhacs, M. Chaker, and B. J. Siwick, A photoinduced metal-like phase of monoclinic vanadium dioxide revealed by ultrafast electron diffraction, Science **346**, 445 (2014).

[14] T. Ishikawa, S. A. Hayes, S. Keskin, G. Corthey, M. Hada, K. Pichugin, A. Marx, J. Hirscht, K. Shionuma, K. Onda *et al.*, Direct observation of collective modes coupled to molecular orbital-driven charge transfer, Science **350**, 1501 (2015).

[15] Y. Jiang, L. C. Liu, H. Müller-Werkmeister, C. Lu, D. Zhang, R. L. Field, A. Sarracini, G. Moriena, E. Collet, and R. J. D. Miller, Structural dynamics upon photoexcitation in a spin crossover crystal probed with femtosecond electron diffraction, Angew. Chem. Int. Ed. **56**, 7130 (2017).

[16] M. Gao, C. Lu, H. Jean-Ruel, L. C. Liu, A. Marx, K. Onda, S. Koshihara, Y. Nakano, X. Shao, T. Hiramatsu *et al.*, Mapping molecular motions leading to charge delocalization with ultrabright electrons, Nature **496**, 343 (2013).

[17] N. Erasmus, M. Eichberger, K. Haupt, I. Boshoff, G. Kassier, R. Birmurske, H. Berger, J. Demsar, and H. Schwoerer, Ultrafast Dynamics of Charge Density Waves in $4H_b$-$TaSe_2$ Probed by Femtosecond Electron Diffraction, Phys. Rev. Lett. **109**, 167402 (2012).

[18] S. Vogelgesang, G. Storeck, J. G. Horstmann, T. Diekmann, M. Sivis, S. Schramm, K. Rossnagel, S. Schäfer, and C. Ropers, Phase ordering of charge density waves traced by ultrafast low-energy electron diffraction, Nat. Phys. **14**, 184 (2018).

[19] H. Ihee, V. A. Lobastov, U. M. Gomez, B. M. Goodson, R. Srinivasan, C. Y. Ruan, and A. H. Zewail, Direct imaging of transient molecular structures with ultrafast diffraction, Science **291**, 458 (2001).

[20] J. Yang, M. Guehr, X. Shen, R. Li, T. Vecchione, R. Coffee, J. Corbett, A. Fry, N. Hartmann, C. Hast *et al.*, Diffractive Imaging of Coherent Nuclear Motion in Isolated Molecules, Phys. Rev. Lett. **117**, 153002 (2016).

[21] M. Eichberger, N. Erasmus, K. Haupt, G. Kassier, A. von Flotow, J. Demsar, and H. Schwoerer, Femtosecond streaking of electron diffraction patterns to study structural dynamics in crystalline matter, Appl. Phys. Lett. **102**, 121106 (2013).

[22] P. Musumeci, J. T. Moody, C. M. Scoby, M. S. Gutierrez, M. Westfall, and R. K. Li, Capturing ultrafast structural evolutions with a single pulse of MeV electrons: Radio frequency streak camera based electron diffraction, J. Appl. Phys. **108**, 114513 (2010).

[23] D. S. Badali and R. J. D. Miller, Robust reconstruction of time-resolved diffraction from ultrafast streak cameras, Struct. Dyn. **4**, 054302 (2017).

[24] A. J. McCulloch, D. V. Sheludko, M. Junker, and R. E. Scholten, High-coherence picosecond electron bunches from cold atoms, Nat. Commun. **4**, 1692 (2013).

[25] G. H. Kassier, K. Haupt, N. Erasmus, E. G. Rohwer, H. M. von Bergmann, H. Schwoerer, S. M. M. Coelho, and F. D. Auret, A compact streak camera for 150 fs time resolved measurement of bright pulses in ultrafast electron diffraction, Rev. Sci. Instrum. **81**, 105103 (2010).

[26] J. M. Bioucas-Dias and M. A. T. Figueiredo, A new TwIST: Two-step iterative shrinkage/ thresholding algorithms for image reconstruction, IEEE Trans. Image Process. **16**, 2992 (2007).

[27] B. J. Siwick, J. R. Dwyer, R. E. Jordan, and R. J. D. Miller, Ultrafast electron optics: Propagation dynamics of femtosecond electron packets, J. Appl. Phys. **92**, 1643 (2002).

[28] W. J. Engelen, M. A. van der Heijden, D. J. Bakker, E. J. D. Vredenbregt, and O. J. Luiten, High-coherence electron bunches produced by femtosecond photoionization, Nat. Commun. **4**, 1693 (2013).

[29] D. Zhang, A. Fallahi, M. Hemmer, X. Wu, M. Fakhari, Y. Hua, H. Cankaya, A. Calendron, L. E. Zapata, N. H. Matlis, and F. X. Kärtner, Segmented terahertz electron accelerator and manipulator (STEAM), Nat. Photonics **12**, 336 (2018).